Anticancer potency of novel organometallic Ir(III) complexes with phosphines derived from fluoroquinolones encapsulated in polymeric micelles

Sandra Kozieł,[a] Urszula K. Komarnicka,*[a] Aleksandra Ziółkowska,[a] Agnieszka Skórska-Stania,[b] Barbara Pucelik,[c] Michał Płotek,[b,d] Victor Sebastian[e,f], Alina Bieńko,[a] Grażyna Stochel,[b] and Agnieszka Kyzioł*[b]

[a.] *Faculty of Chemistry, University of Wroclaw, Joliot-Curie 14, 50-383 Wroclaw, Poland*
[b.] *Faculty of Chemistry, Jagiellonian University in Krakow, Gronostajowa 2, 30-387 Krakow, Poland*
[c.] *Małopolska Centre of Biotechnology, Jagiellonian University, Gronostajowa 7A, 30-387, Kraków, Poland.*
[d.] *Faculty of Conservation and Restoration of Works of Art, Jan Matejko Academy of Fine Arts in Krakow, Lea 27-29, 30-052 Krakow, Poland*
[e.] *Departmentof Chemical Engineering, Aragon Institute of Nanoscience (INA),The Aragón Materials Science Institute (ICMA), University of Zaragoza, Campus Río Ebro-Edificio I+D, Mariano Esquillor S/N, 50018 Zaragoza, Spain*
[f.] *Networking Research Center on Bioengineering, Biomaterials and Nanomedicine, CIBER-BBN, 28-029 Madrid, Spain*

Corresponding author e-mail address:urszula.komarnicka@chem.uni.wroc.pl, kyziol@chemia.uj.edu.pl

Graphical abstract

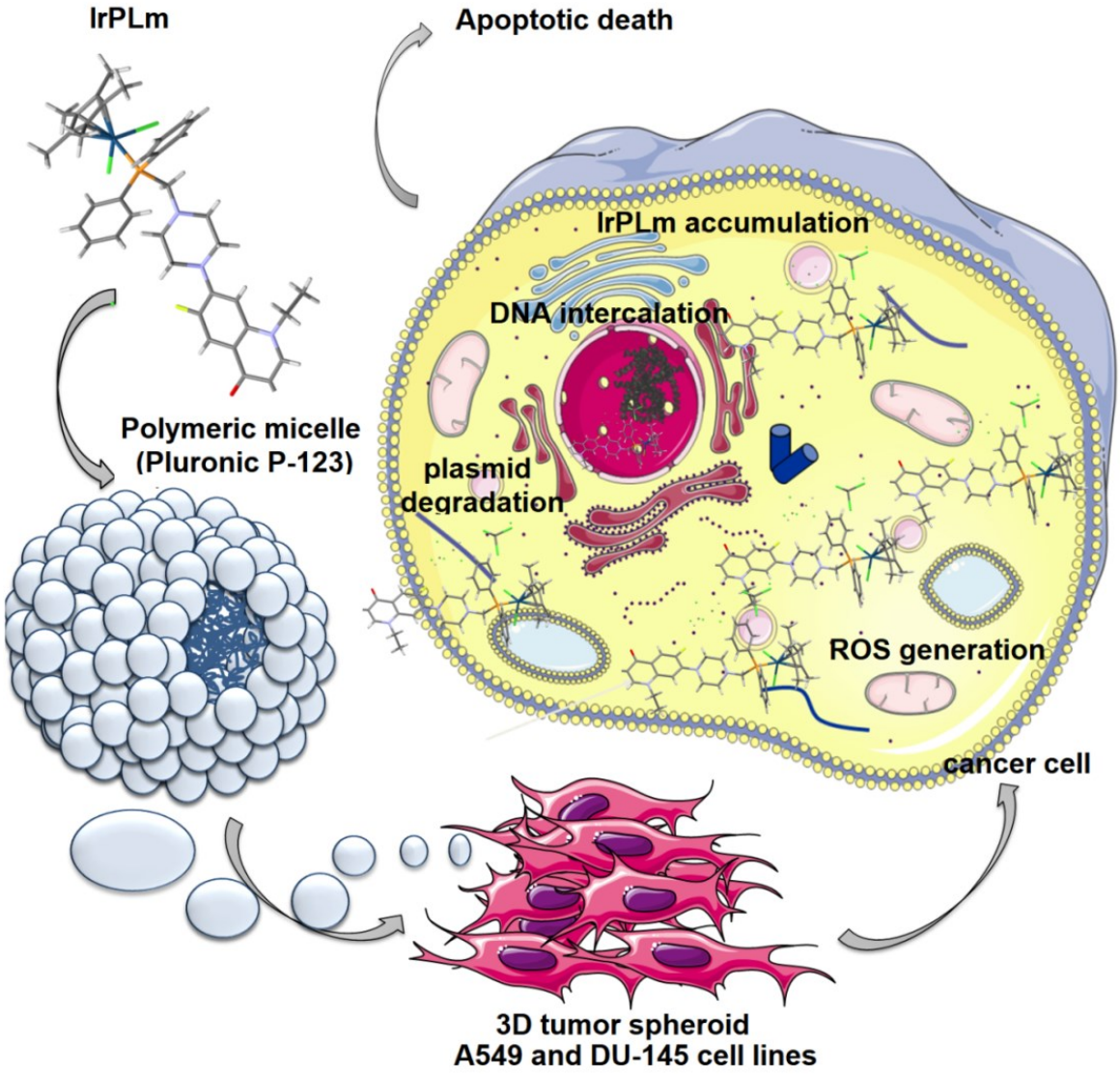

Table S1. Crystallographic experimental details.

Parameters	**IrPCp**·$CHCl_3$	**IrPLm**·1.5$CHCl_3$	**IrPNr**·2$CHCl_3$
Moiety formula	$IrCl_5PN_3O_3C_{41}H_{45}$	$IrCl_{6.5}PN_3O_3C_{41.5}H_{46.5}$	$IrCl_8PN_3O_3C_{41}H_{46}$
Formula weight ($g \cdot mol^{-1}$)	1047.22	1126.91	1154.58
Crystal description	yellow plate	light orange plate	yellow prism
Crystal size (mm)	0.20 x 0.20 x 0.02	0.10 x 0.10 x 0.05	0.30 x 0.30 x 0.20
Temperature (K)	130	100	130
Type of radiation	Cu *K*α	Mo *K*α	Cu *K*α
Crystal system	Triclinic	Monoclinic	Monoclinic
Space group	P $\bar{1}$	I 2/a	P 2_1/n
a (Å)	9.0544(4)	24.6249(3)	10.1356(2)
b (Å)	11.8197(5)	8.35470(1)	17.3727(3)
c (Å)	20.8951(8)	44.3459(5)	25.6237(4)
α (°)	85.841(3)	90	90
β (°)	86.837(3)	104.3440(1)	93.1370(1)°
γ (°)	67.930(4)	90	90
Volume ($Å^3$)	2065.94(16)	8839.03(18)	4505.13(14)
Z	2	8	4
Density calc. (g/cm^3)	1.683	1.694	1.702
Absorption coeff. (mm^{-1})	9.983	3.501	10.818
F(000)	1044	4488	2296
$\theta_{min} - \theta_{max}$ (°)	4.042 to 71.700	2.215 to 31.772	3.075 to 71.574
hkl range	-11 ← h ← 11 -14 ← k ← 14 -25 ← l ← 25	-32 ← h ← 35 -11 ← k ← 11 -63 ← l ← 64	-12 ← h ← 12 -21 ← k ← 21 -31 ← l ← 31
Reflections collected	28428	154041	69550
Independent reflections	7969	13616	8730
R_{int}	0.0886	0.0395	0.1085
Completeness to θ_{full} (%)	99.9	99.9	99.8
Absorption correction type	multi-scan	multi-scan	multi-scan
T_{max} and T_{min}	1.000 and 0.219	1.000 and 0.871	1.000 and 0.158
Data/restraints/parameters	7969 / 0 / 504	13616 / 3 / 541	8730 / 0 / 533
Goodness of fit F^2	1.026	1.059	1.108
R_1, wR_2 [I>2σ(I)]	0.0440, 0.1081	0.0321, 0.0716	0.0642, 0.1514
R_1, wR_2 (all data)	0.0544, 0.1169	0.0394, 0.0734	0.0710, 0.1560
Largest diff. peak and hole (e $Å^{-3}$)	1.919 -1.931	3.325, -0.922	2.658, -2.947

Table S2. Selected bond lengths (Å) and angles (°) for crystallized complexes.

	IrPCp·$CHCl_3$	**IrPLm**·$1.5CHCl_3$	**IrPNr**·$2CHCl_3$
C^1-C^5	1.428(8)	1.403(5)	1.447(12)
C^1-C^2	1.432(8)	1.450(5)	1.420(13)
C^2-C^3	1.455(8)	1.431(4)	1.422(14)
C^3-C^4	1.410(8)	1.429(4)	1.439(13)
C^4-C^5	1.457(8)	1.454(4)	1.434(12)
$C_{(Cp*ring)}$-$C_{(Cp*CH_3)}$	0.9600	1.495(8)	0.9600
Ir^1–C^1	2.159(5)	2.226(3)	2.226(8)
Ir^1–C^2	2.153(5)	2.169(3)	2.219(8)
Ir^1–C^3	2.251(5)	2.172(3)	2.158(9)
Ir^1–C^4	2.236(5)	2.149(3)	2.179(8)
Ir^1–C^5	2.177(5)	2.235(3)	2.139(8)
Ir^1–C_{Cp*}(average)	2.219(5)	2.190(2)	2.184(2)
Ir^1–Ccentroid	1.824	1.820	1.814
Ir^1–P^1	2.2919(1)	2.308(6)	2.310(6)
Ir^1–Cl^1	2.4195(1)	2.418(6)	2.411(6)
Ir^1–Cl^2	2.4114(1)	2.408(6)	2.416(2)
P^1–C^{11}	1.863(5)	1.854(3)	1.864(8)
P^1–C^{41}	1.827(5)	1.814(3)	1.817(8)
P^1–C^{51}	1.823(5)	1.826(3)	1.835(8)
P^1–Ir^1–Cl^1	90.45(5)	90.18(2)	89.43(7)
P^1–Ir^1–Cl^2	90.03(4)	86.75(2)	86.77(7)
Cl^1–Ir^1–Cl^2	86.04(4)	87.52(2)	89.45(8)
Ccentroid–Ir^1–P^1	129.78	132.99	132.93
Ccentroid–Ir^1–Cl^1	124.56	123.04	132.93
Ccentroid–Ir^1–Cl^2	123.42	123.13	132.93
Ir^1–P^1–C^{11}	116.34(17)	111.27(9)	112.1(2)
Ir^1–P^1–C^{41}	111.59(18)	116.09(9)	116.4(3)
Ir^1–P^1–C^{51}	115.83(18)	106.68(12)	111.0(3)
C^{11}–P^1–C^{41}	100.4(2)	103.49(12)	107.1(4)
C^{11}–P^1–C^{51}	101.2(2)	103.49(12)	104.8(4)
C^{41}–P^1–C^{51}	110.1(2)	106.10(12)	104.6(4)

Ccentroid – center of gravity of cyclopentadienyl anion;
Ir^1–C_{Cp*} (average) – average calculated from: Ir^1–C^1, Ir^1–C^2, Ir^1–C^3, Ir^1–C^4, Ir^1-C^5
$C_{(Cp*ring)}$-$C_{(Cp*CH_3)}$ – average calculated from: C^1-C^{1A}, C^2-C^{2A}, C^3-C^{3A}, C^4-C^{4A}, C^5-C^{5A}

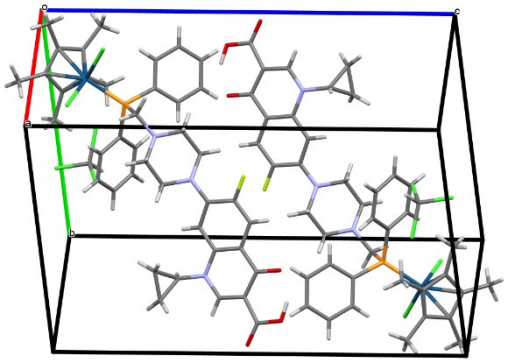

IrPCp·$CHCl_3$

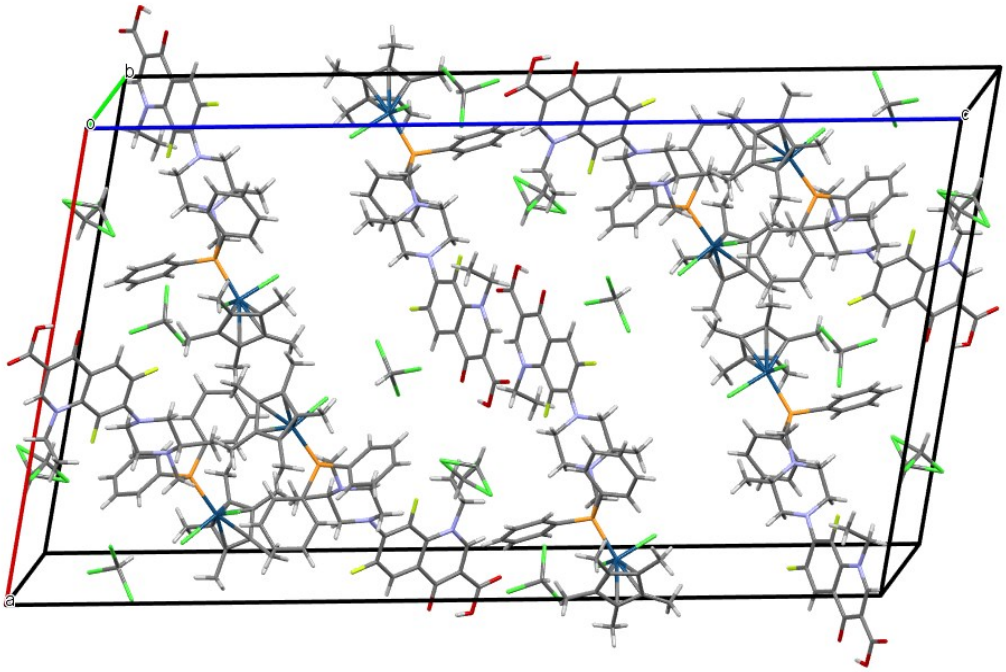

IrPLm·1.5$CHCl_3$

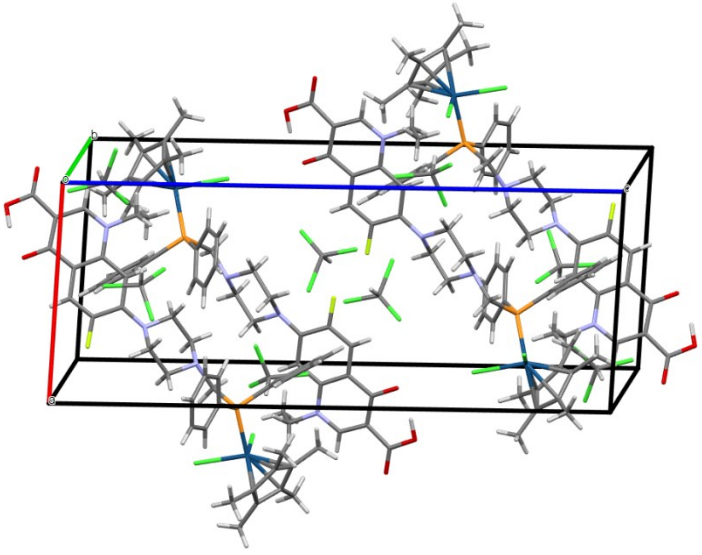

IrPNr·2$CHCl_3$

Fig. S1. The best view of crystal cells of **IrPCp**·$CHCl_3$, **IrPLm**·1.5$CHCl_3$ and **IrPNr**·2$CHCl_3$, respectively.

Table S3. Cumulative NMR data for ligands and iridium-complexes.

	Dimer Ir	**PCp** [1]	**PSf** [2]	**PLm** [3]	**PNr** [4]	**IrPCp**	**IrPSf**	**IrPLm**	**IrPNr**
P[1]		**-27.4**	**-35.9**	**-28.8**	**-27.5**	**-1.30**	**-3.06**	**-1.82**	**-1.38**
H[1]	1.69 s					1.35 d (2.2)	1.33 d (2.2)	1.34 d (2.2)	1.35 d (2.2)
H[11]		3.29 d (2.9)	3.93 bs	2.80 bs	3.29 d (2.8)	4.07 s	4.25 s	4.15 dd (40.0;16.0)	4.07 s
H[12, 15]		3.37	3.20 m	2.95-3.45	3.36 m	2.99 bt (4.8)	2.45 m	2.14-3.14 m	2.97 bt (4.6)
H[13, 14]		2.90	3.93 m		2.89 m	2.39 bt (4.8)	2.80-3.07 m		2.39 bt (4.6)
H[16]			0.94 d (5.9)	0.97 d (5.7)			0.72 d (6.4)	0.62 d (6.3)	
H[17]									
H[42]		7.34-7.47	7.29-7.65	7.03-7.60	7.33-7.46	8.00-8.11 m	7.98-8.13 m	7.99-8.15 m	8.00-8.11 m
H[43, 44]						7.44-7.53 m	7.43-7.51 m	7.39-7.56 m	7.42-7.54 m
H[63]		7.95 d (13.8)	6.46 bs	7.84 d (11.4)	7.95 d (13.0)	7.92 d (13.3)	6.41 bd	7.87 dd (12.0; 1.7)	7.96 d (13.2)
H[67]		8.71 s	8.62 s	8.52 s	8.63 s	8.72 s	8.61 s	8.55 s	8.62 s
H[69]		7.34-7.47			6.82 d (6.8)	7.16 d (7.1)			6.64 d (6.9)
H[70]		15.01 s	14.54 bs	14.65 bs	15.13 bs	15.02 s	14.65 bs	14.68 s	15.09 s
H[71]		3.53 m	3.93 bs	4.39 d (3.6)	4.31 m	3.47 m	3.87 m	4.40 qd (7.2; 3.3)	4.25 q (7/2)
H[72]		1.18 m	1.07-1.21 m	1.48 t (3.7)	1.56 m	1.11-1.33 m	1.04-1.20 m	1.50 t (7.0)	1.54 t (7.3)
H[73]									

[1] A. Bykowska, R. Starosta, A. Brzuszkiewicz, B. Bażanów, M. Florek, N. Jackulak, J. Król, J. Grzesiak, K. Kaliński, M. Jeżowska-Bojczuk, *Polyhedron*, 2013, **60**, 23-29.

[2] U. K. Komarnicka, R. Starosta, K. Guz-Regner, G. Bugla-Płoskońska, A. Kyzioł, M. Jeżowska-Bojczuk, *J. Mol. Struct.*, 2015, **1096**, 55-63.

[3] U. K. Komarnicka, R. Starosta, A. Kyzioł, M. Płotek, M. Puchalska, M. Jeżowska-Bojczuk, *J. Inorg. Biochem.*, 2016, **165**, 25-35.

[4] A. Bykowska, R. Starosta, U. K. Komarnicka, Z. Ciunik, A. Kyzioł, K. Guz-Regner, G. Bugla-Płoskońska, M. Jeżowska-Bojczuk, *New J. Chem.*, 2014, **38**, 1062-1071.

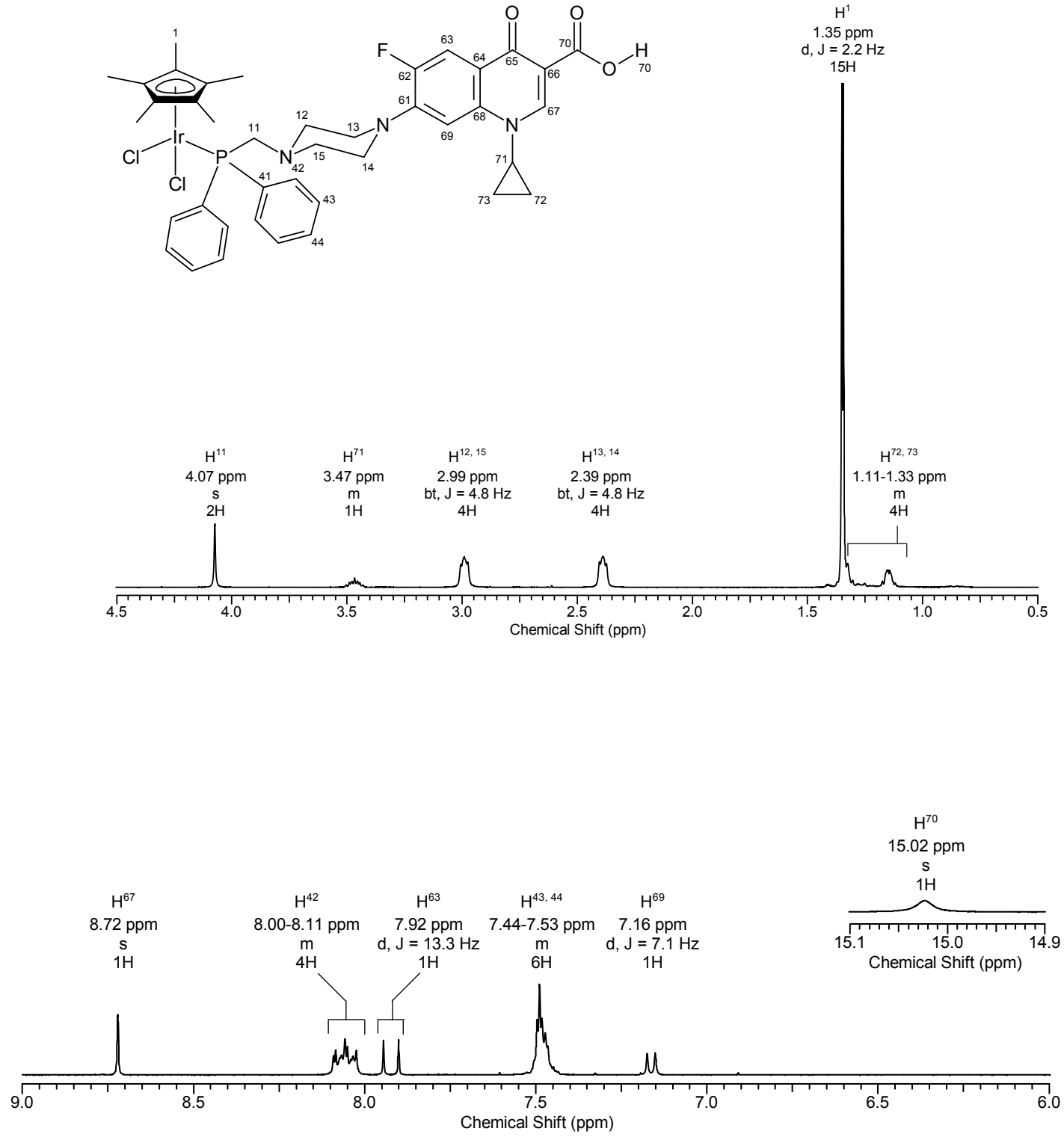

Fig. S2. ^{1}H NMR spectra for **IrPCp** (298 K, $CHCl_3$-d)

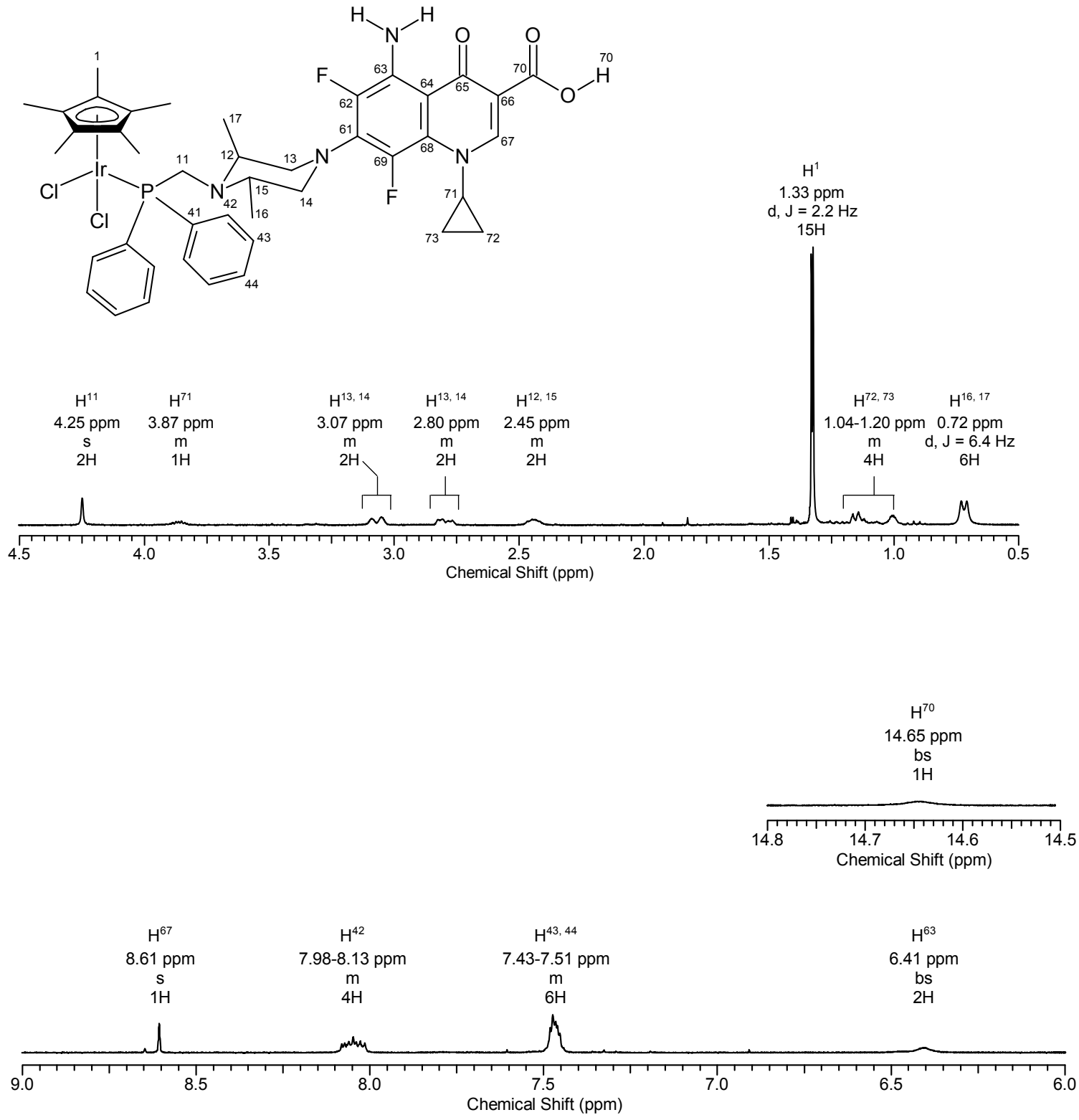

Fig. S3. ^{1}H NMR spectra for **IrPSf** (298 K, $CHCl_3$-d)

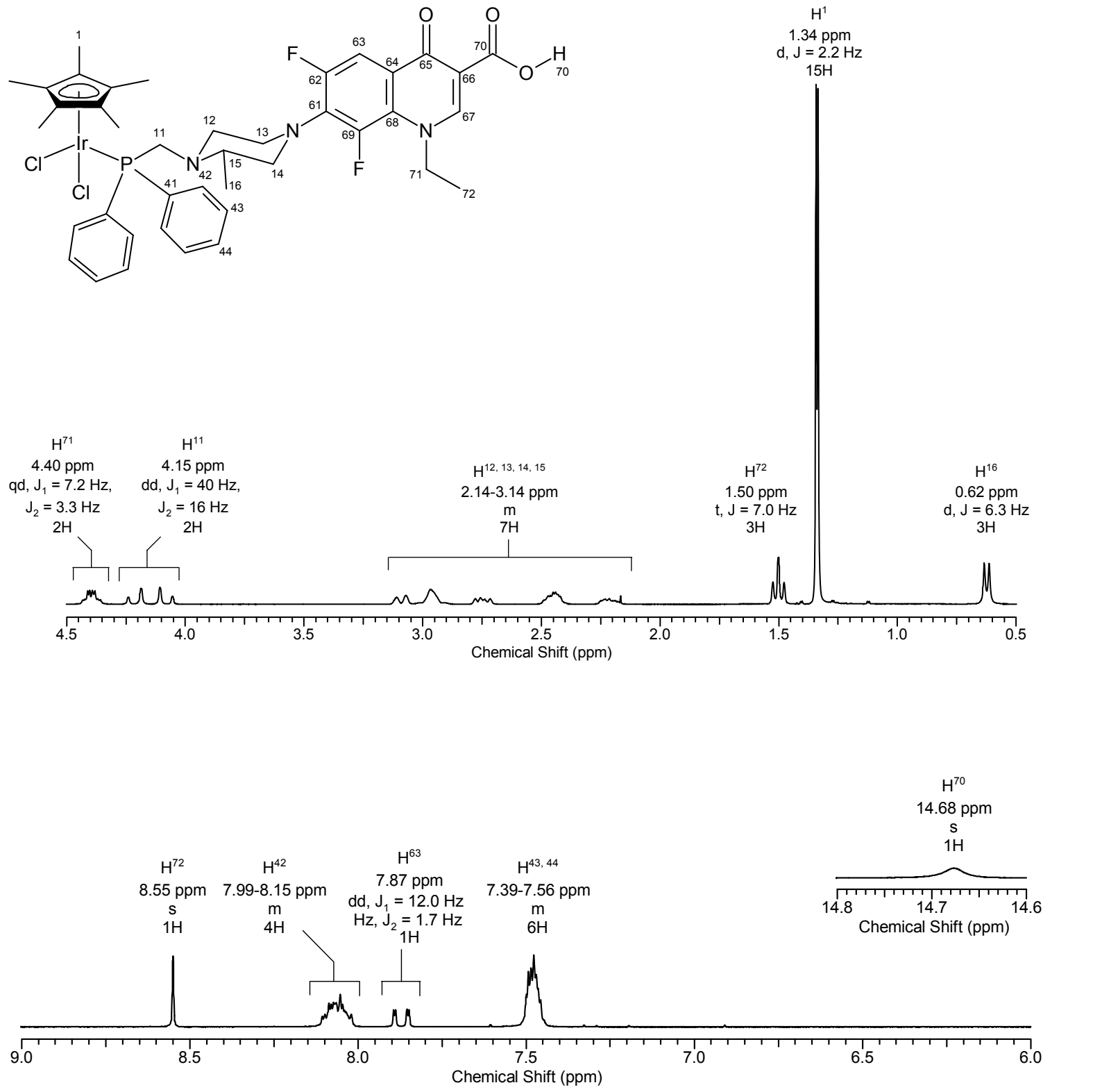

Fig. S4. ^{1}H NMR spectra for **IrPLm** (298 K, $CHCl_3$-d).

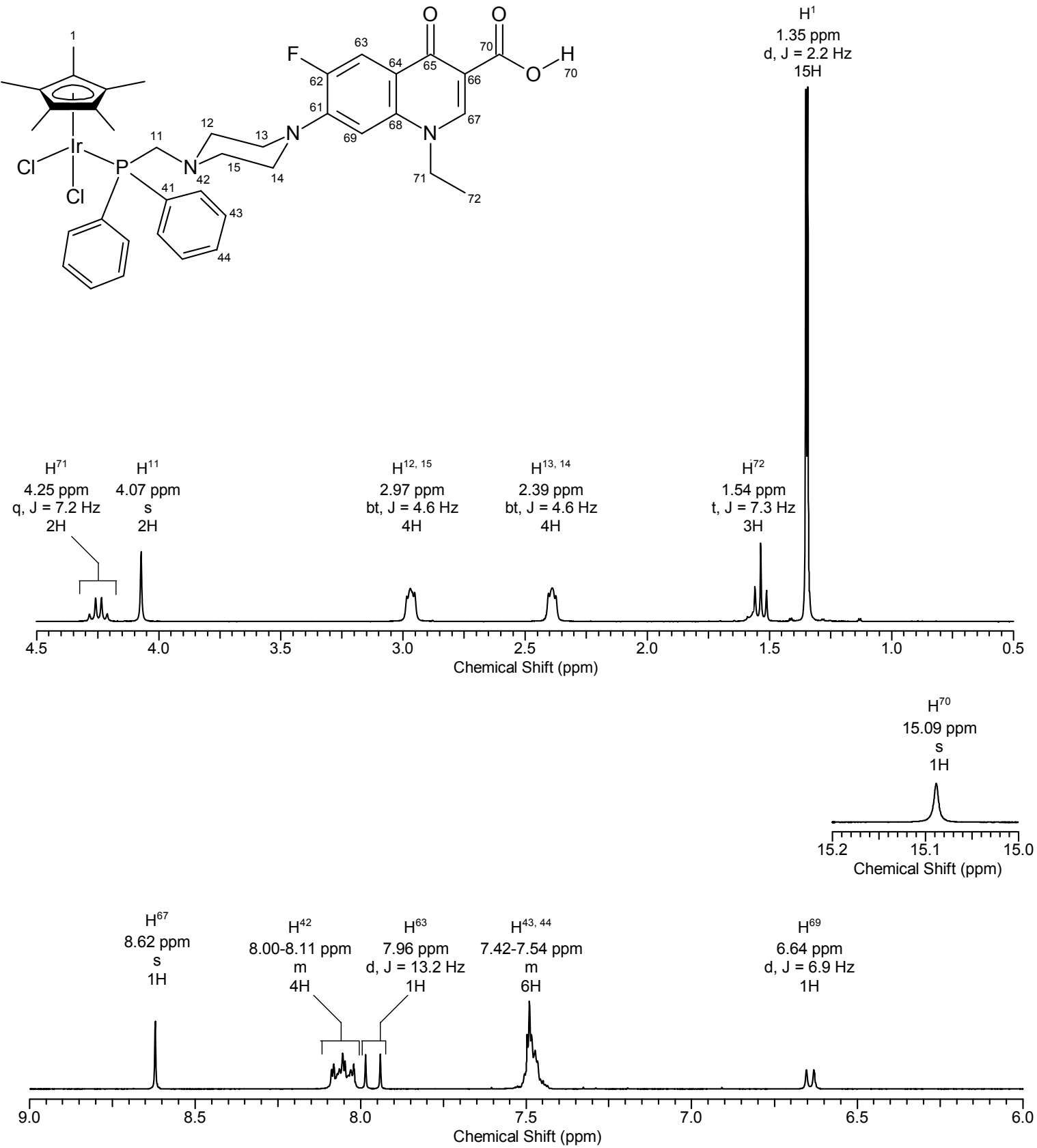

Fig. S5. ^{1}H NMR spectra for **IrPLm** (298 K, $CHCl_3$-d).

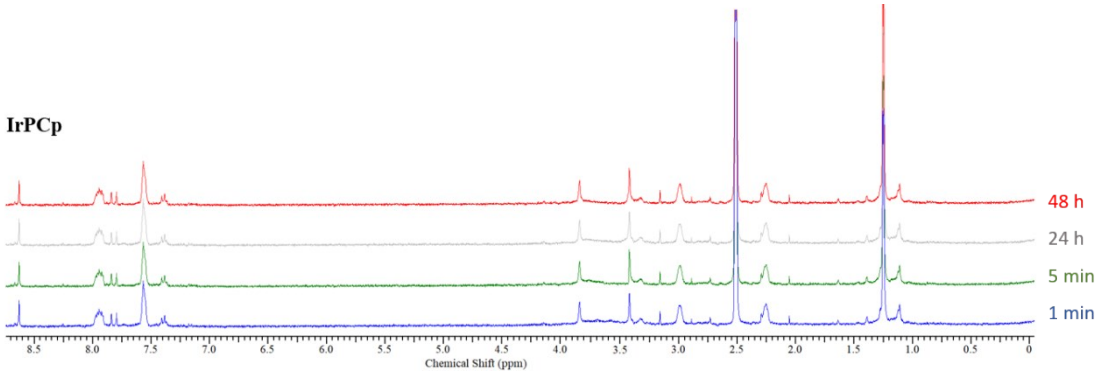

Fig S6. Time-dependent ^{1}H NMR spectroscopic stability study for **IrPCp** in 80% DMSO-d_6/20% D_2O over 48 h.

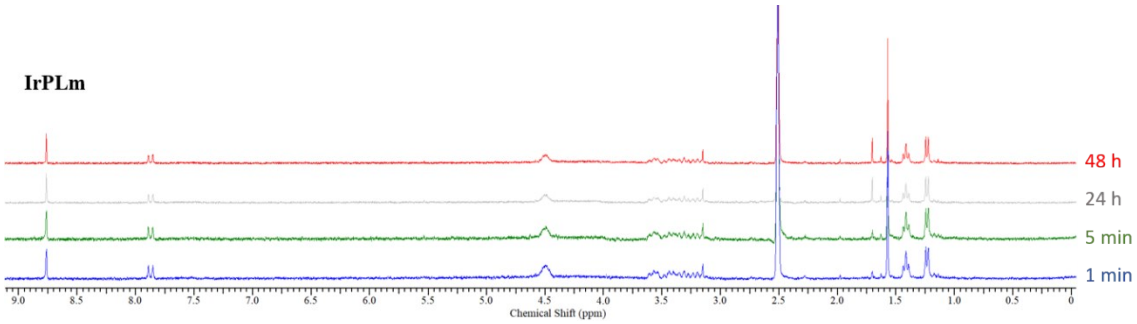

Fig. S7. Time-dependent ^{1}H NMR spectroscopic stability study for **IrPLm** in 70% DMSO-d_6/30% D_2O over 48 h.

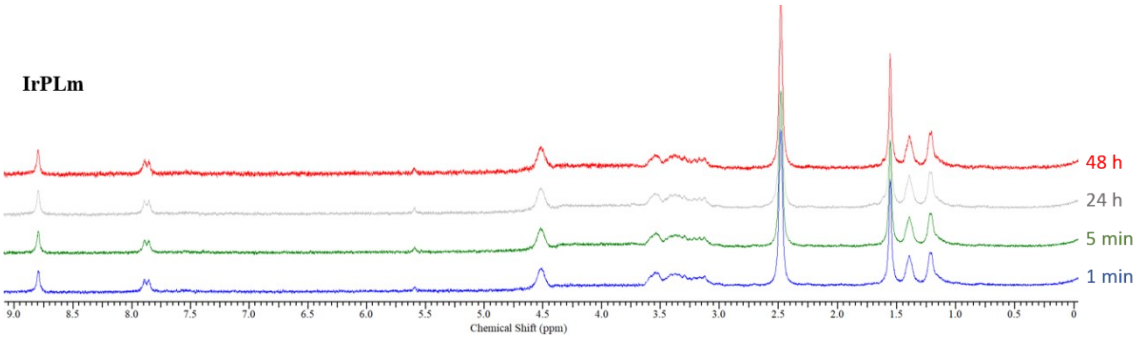

Fig. S8. Time-dependent ^{1}H NMR spectroscopic stability study for **IrPLm** in 80% DMSO-d_6/20% D_2O over 48 h.

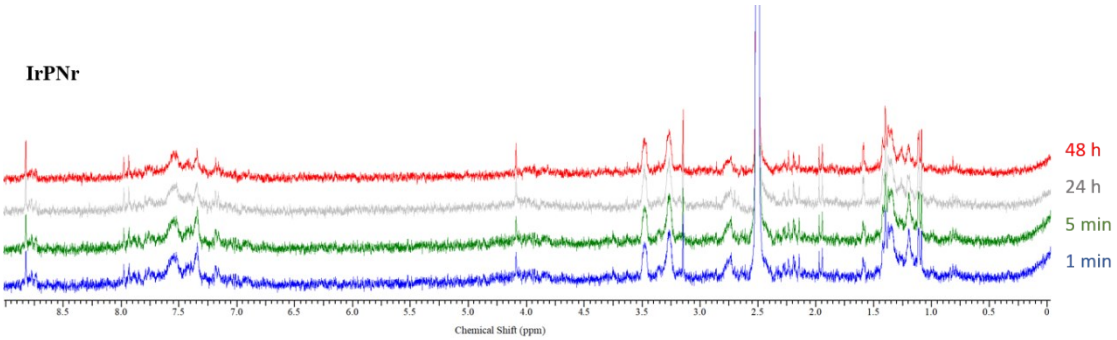

Fig. S9. Time-dependent ^{1}H NMR spectroscopic stability study for **IrPNr** in 70% DMSO-d_6/30% D_2O over 48 h.

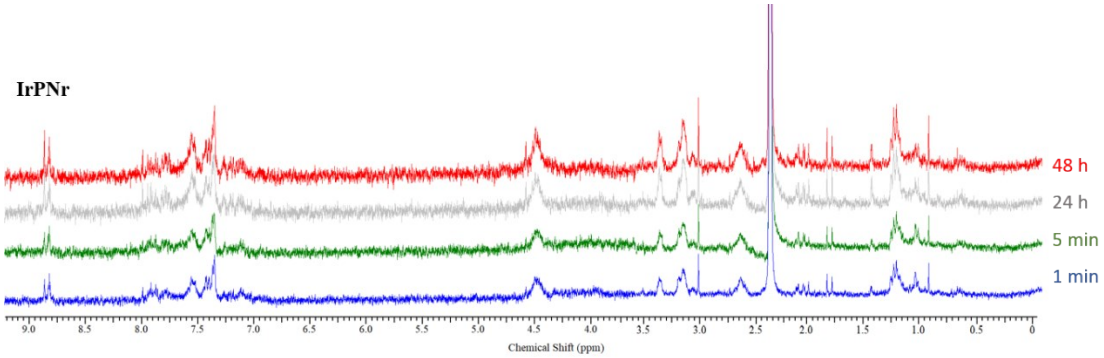

Fig. S10. Time-dependent ^{1}H NMR spectroscopic stability study for **IrPNr** in 80% DMSO-d_6/20% D_2O over 48 h.

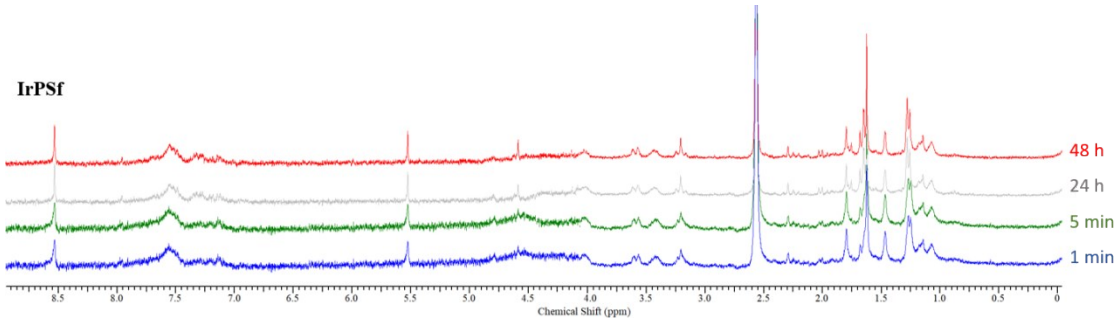

Fig. S11. Time-dependent 1H NMR spectroscopic stability study for **IrPSf** in 70% DMSO-d6/30% D2O over 48 h.

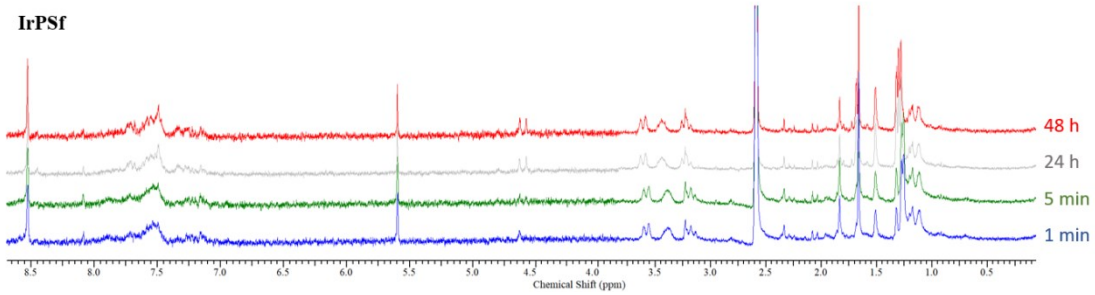

Fig. S12. Time-dependent ^{1}H NMR spectroscopic stability study for **IrPSf** in 80% DMSO-d_6/20% D_2O over 48 h.

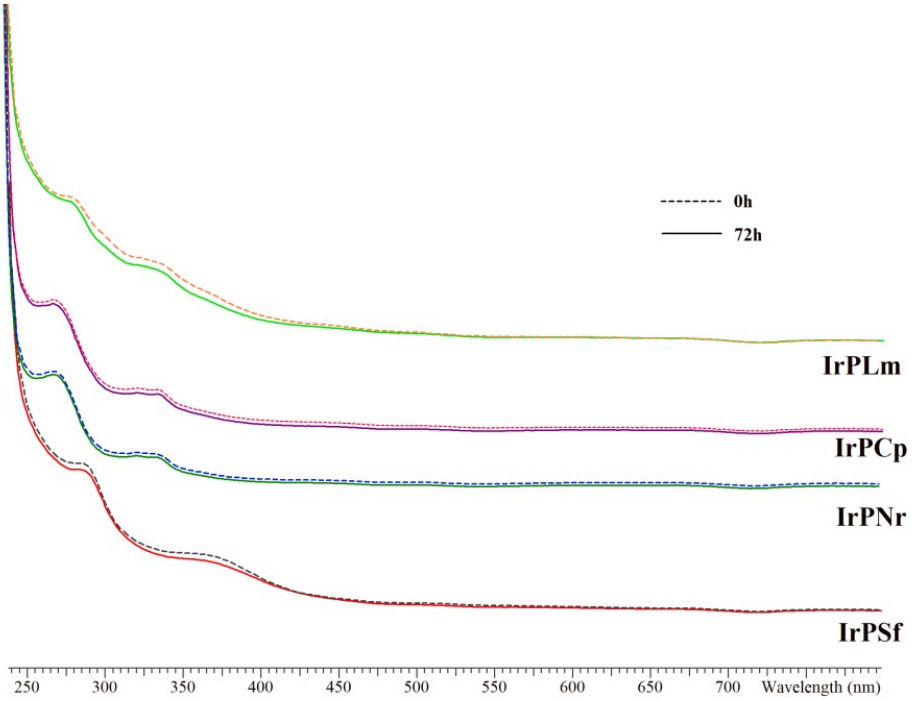

Fig. S13. Stability of the all complexes (**IrPNr**, **IrPLm**, **IrPCp**, **IrPSf)** in cellular medium (DMEM with 2% DMSO; during 72h experiments).

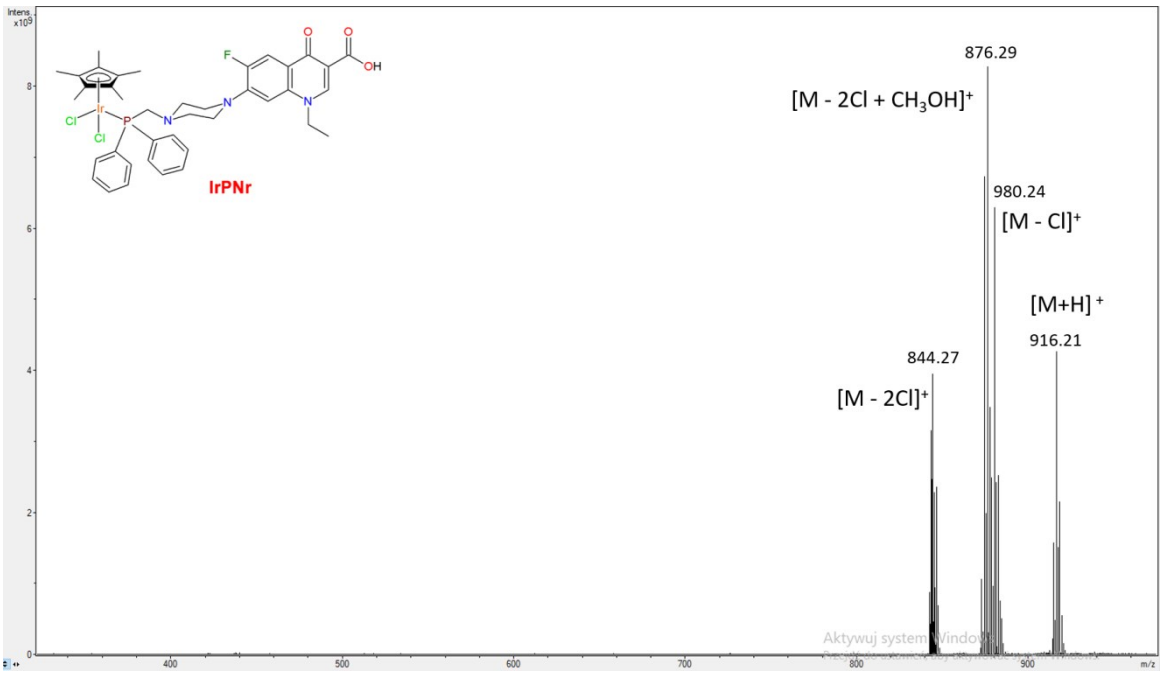

Fig. S14. Full ESI(+)MS spectrum of **IrPNr**.

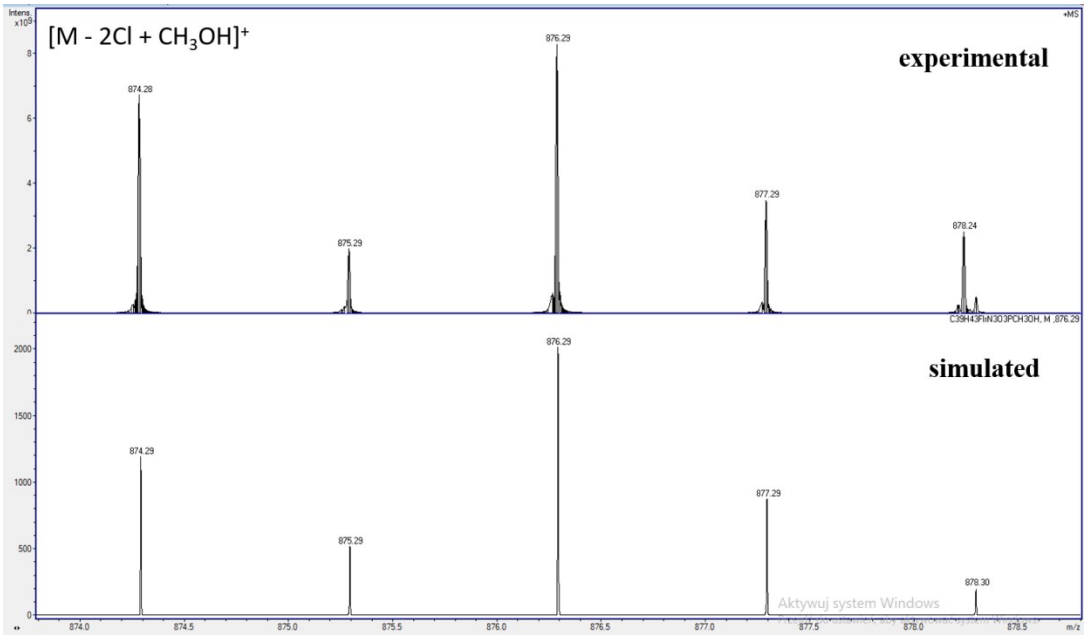

Fig. S15. Experimental and simulated spectra of $[Ir(\eta^5\text{-Cp*})PNr + CH_3OH]^+$

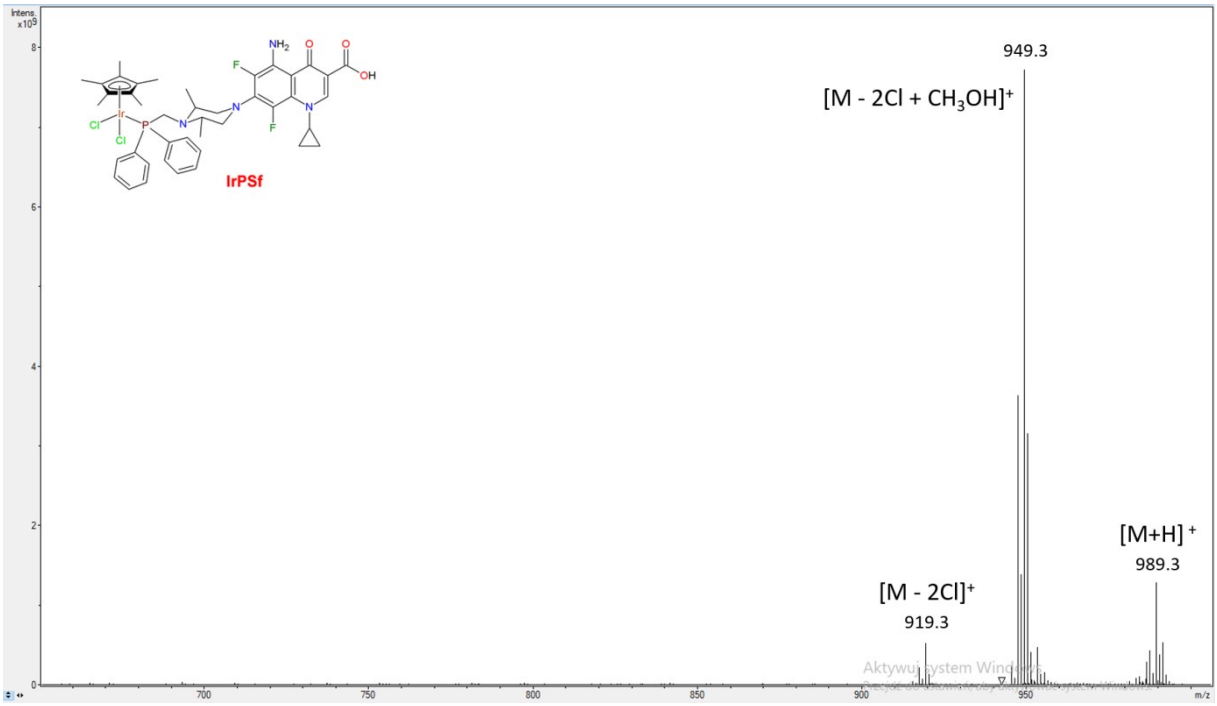

Fig. S16. Full ESI(+)MS spectrum of **IrPSf**.

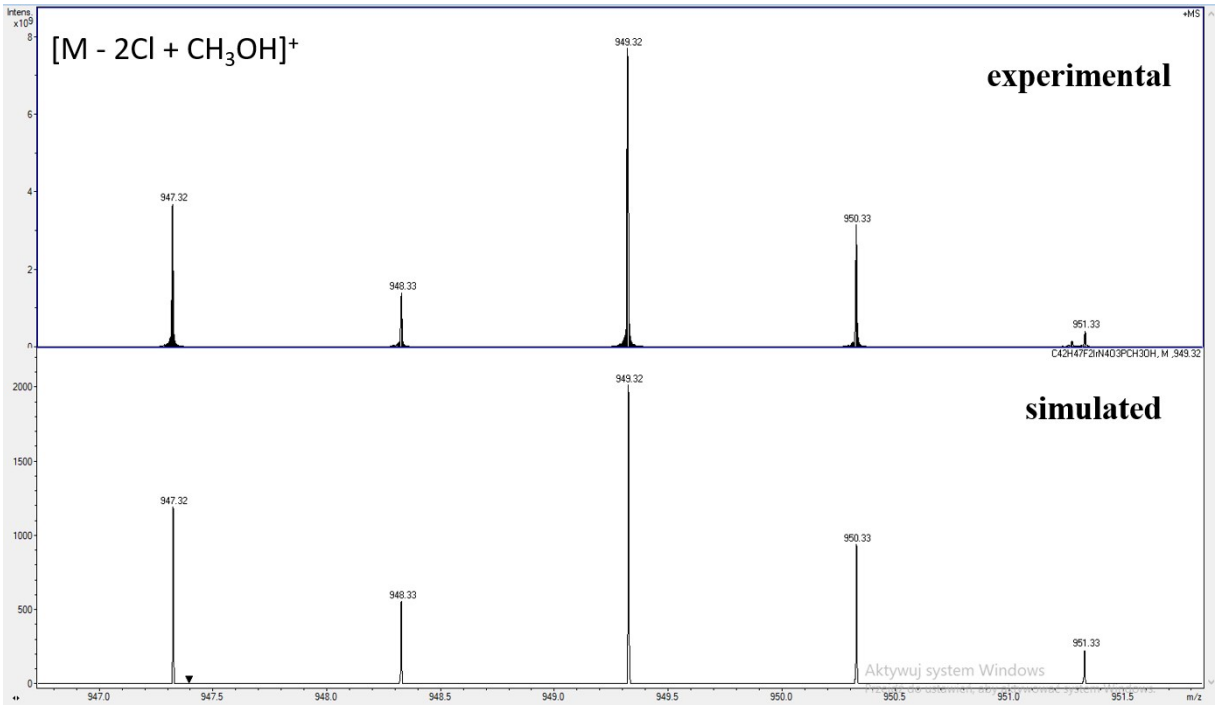

Fig. S17. Experimental and simulated spectra of $[Ir(\eta^5\text{-Cp*})PSf + CH_3OH]^+$

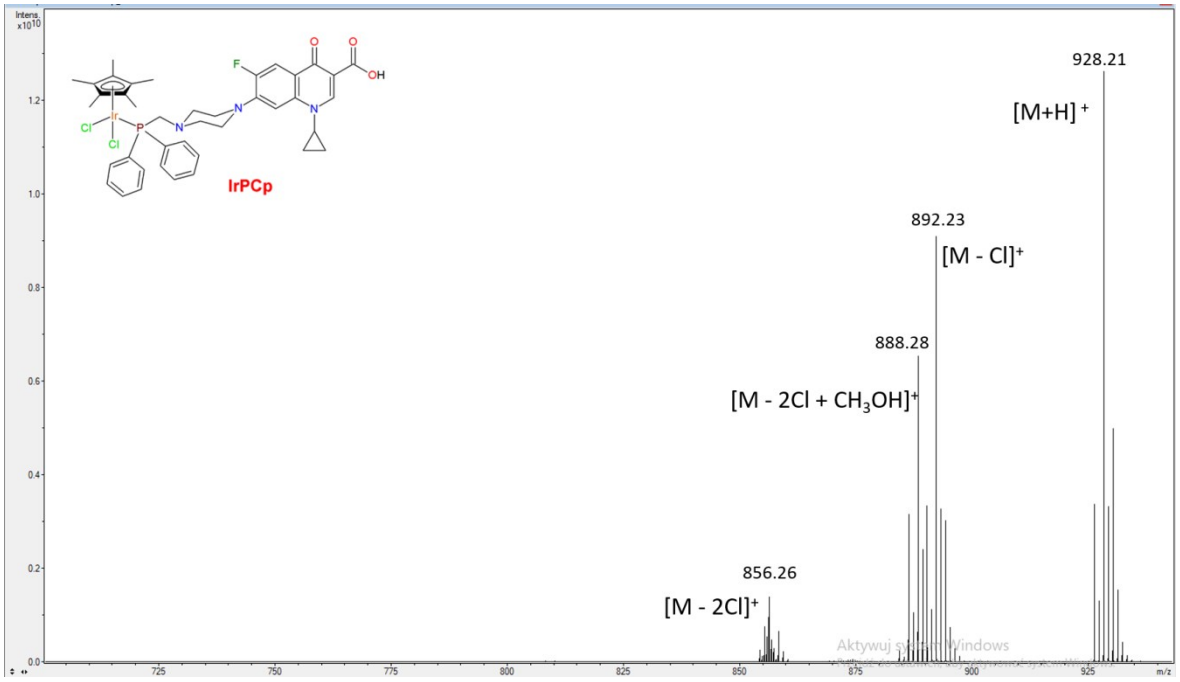

Fig. S18. Full ESI(+)MS spectrum of **IrPCp**.

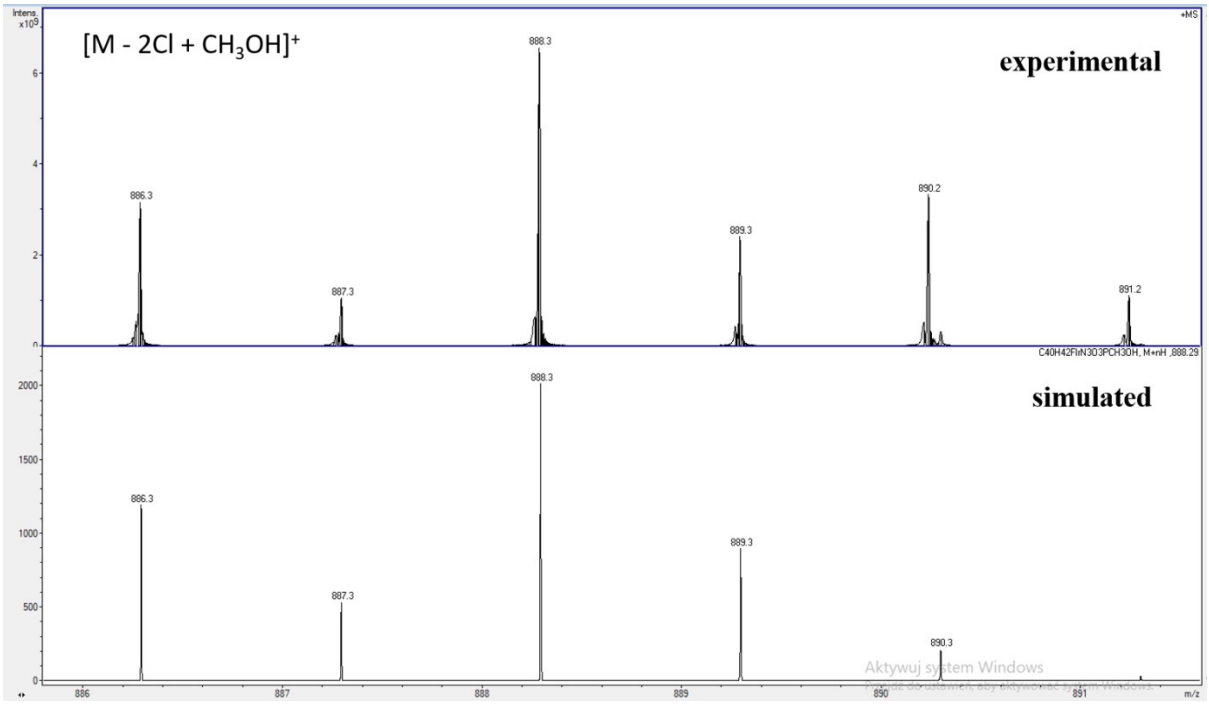

Fig. S19. Experimental and simulated spectra of $[Ir(\eta^5\text{-}Cp^*)PCp + CH_3OH]^+$

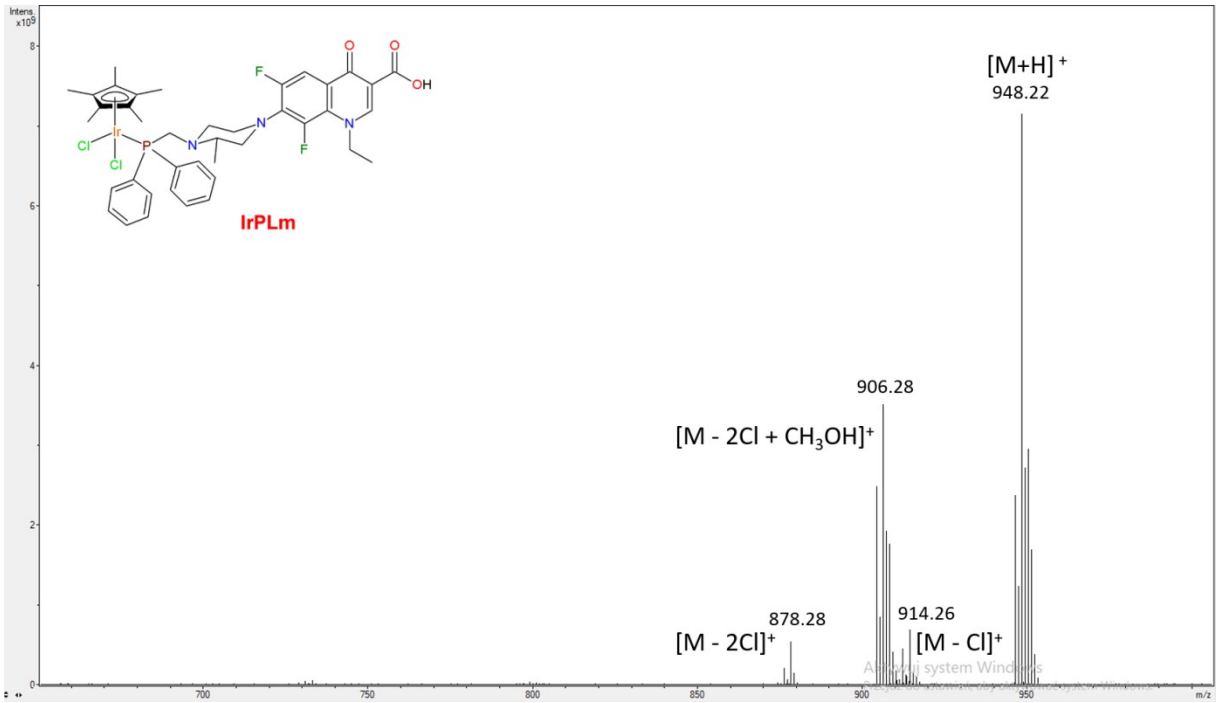

Fig. S20. Full ESI(+)MS spectrum of **IrPLm**.

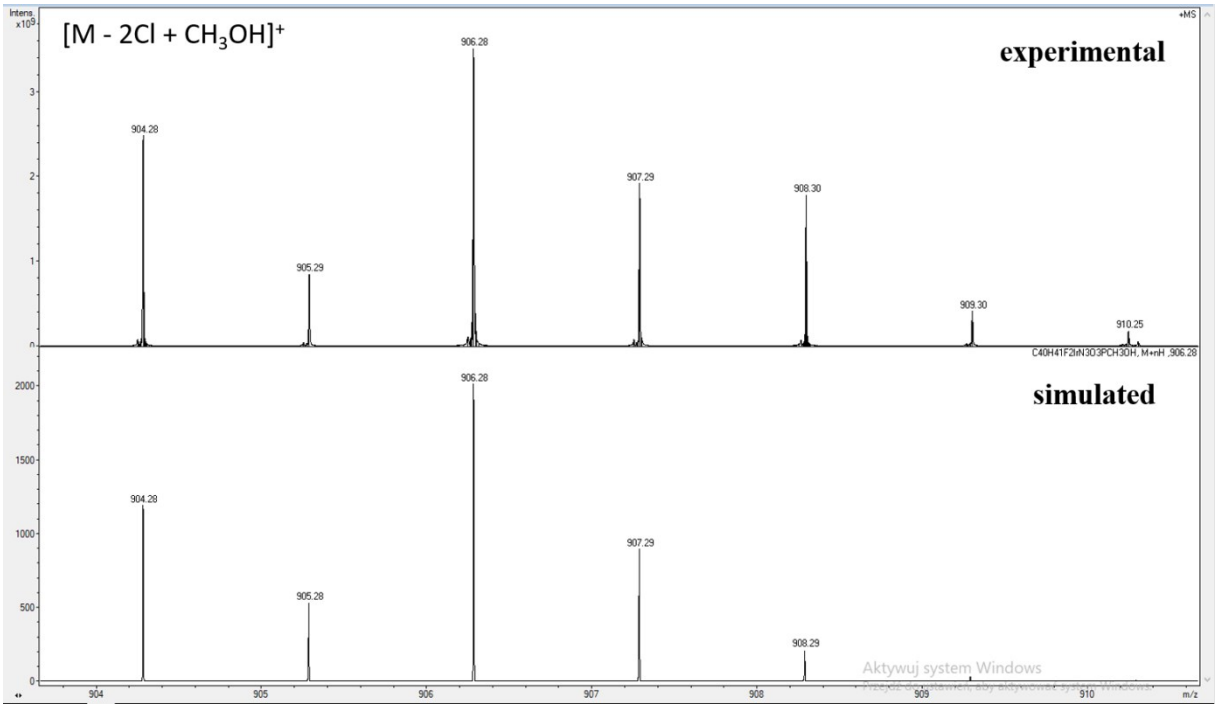

Fig. S21. Experimental and simulated spectra of $[Ir(\eta^5\text{-Cp*})PLm + CH_3OH]^+$

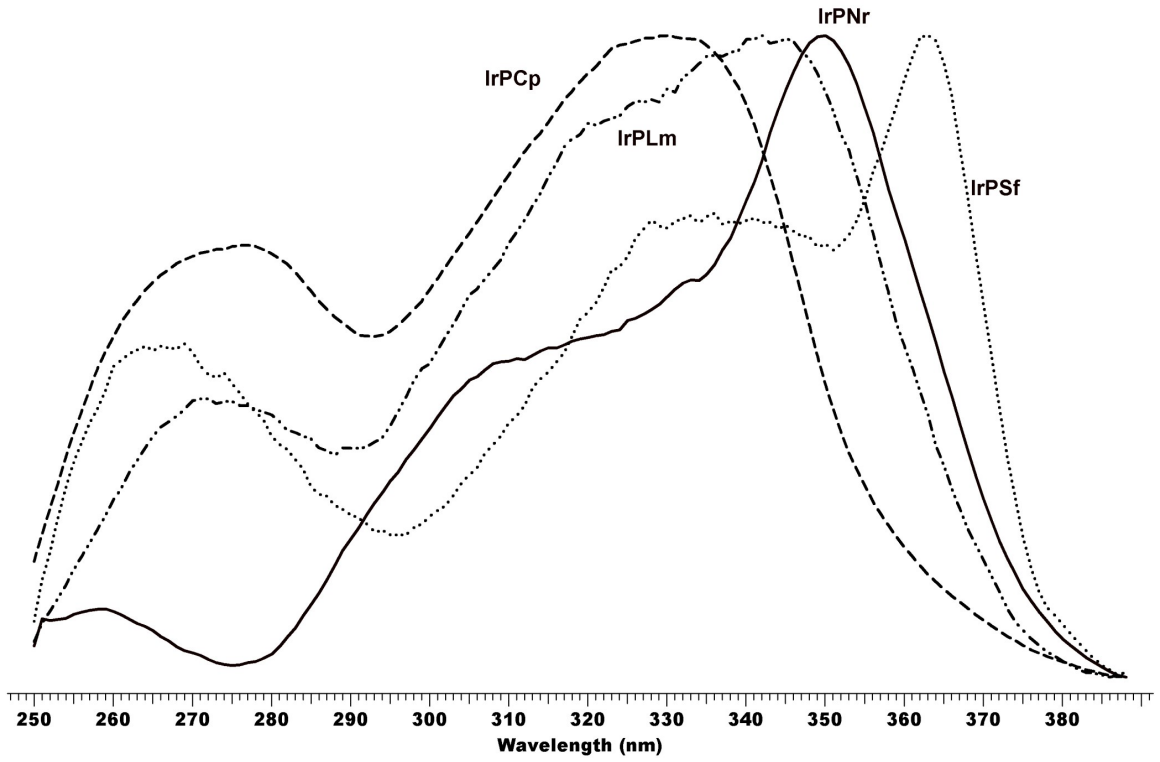

Fig. S22. Excitation spectra of IrPCp, IrPNr, IrPLm and IrPSf

Table S4. Values of IC_{50} [μM] (concentration of a drug required to inhibit the growth of 50% of the cells) for CT26, A549, MCF7, PANC-1, DU-145, HEK293T cells after 24h and 24h + 48h treatment with the studied compounds and cisplatin as reference.

	IC_{50} [μM] ± SD;24h					
	CT26	A549	MCF7	PANC-1	DU-145	HEK293T
IrPCp	-*	68.8±1.7	65.7±2.8	43.0±1.3	11.8±1.1	42.1±2.1
IrPSf	-*	64.8±2.8	61.8±4.1	40.3±4.1	9.1±0.5	44.1±1.2
IrPLm	-*	69.7±4.1	64.5±2.2	48.1±4.3	11.3±0.9	46.0±1.6
IrPNr	-*	71.4±1.6	68.8±5.3	42.6±8.1	12.9±2.1	41.8±1.7
cisplatin	>100	>100	51.9±4.6	>100	>100	21.0±1.8
	IC_{50} [μM] ± SD; 24h + 48h					
IrPCp	6.4±0.3	29.5±0.7	35.0±0.9	8.7±0.3	4.8±0.1	28.5±1.5
IrPSf	4.1±0.7	26.7±1.6	29.3±0.2	7.8±0.6	3.5±0.8	23.0±1.7
IrPLm	5.8±0.2	27.4±1.7	33.7±3.8	8.1±1.1	5.1±0.4	28.0±1.7
IrPNr	5.6±0.4	29.1±1.2	31.7±0.3	8.3±1.3	5.5±0.2	21.4±1.2
cisplatin	80.4± 2.3	71.7±3.7	17.7±8.6	74.5±2.3	65.5±3.6	10.3±2.1

* no available data

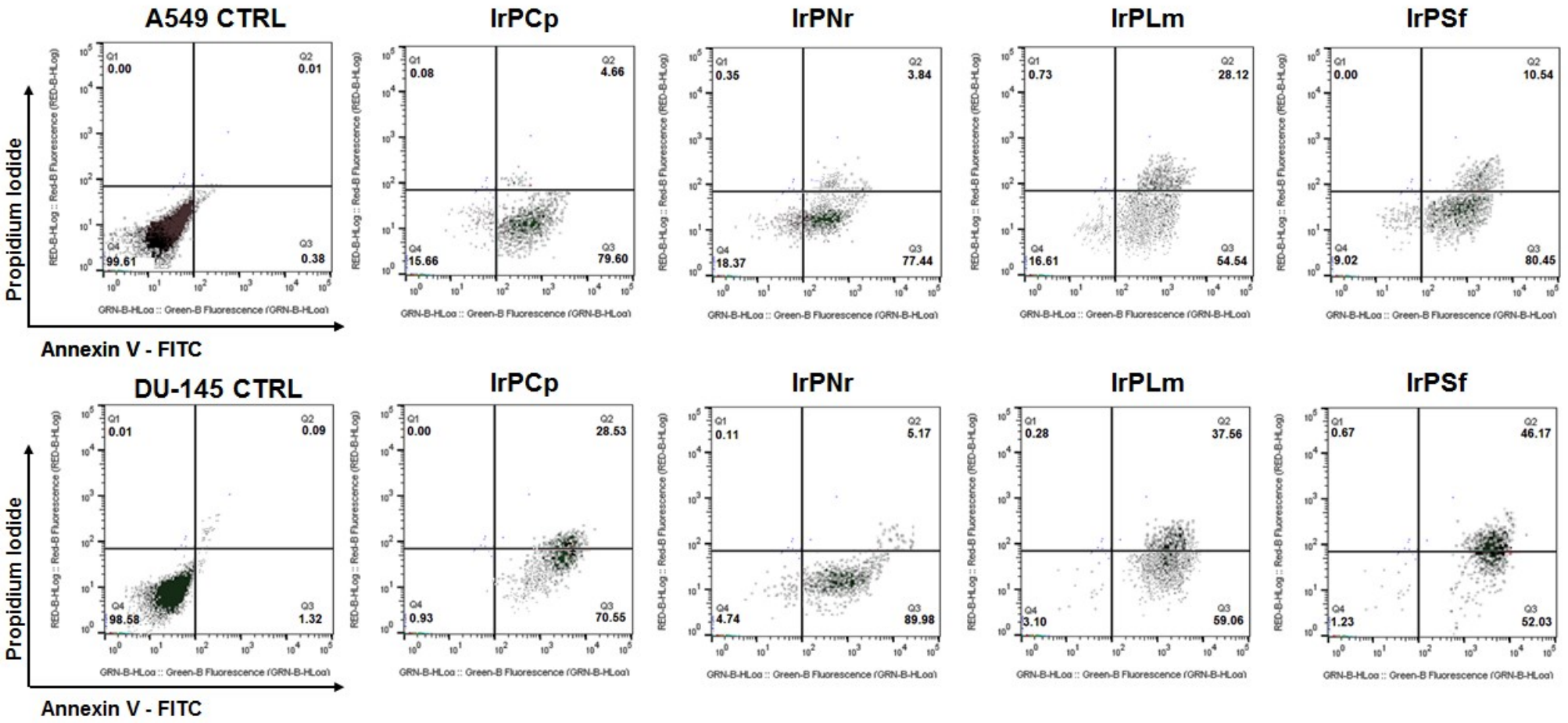

Fig. S23. Percentage analysis [%] of the number live, early/late apoptotic and necrotic cells after 24h + 48h of incubation of A549 and Du-145 cell lines with IrPCp, IrPNr, IrPSf, IrPLm in c = 100 μM. Scatter plots: left bottom – live cells, right bottom – early apoptotic cells, right top – late apoptotic cells, left top – necrotic cells.

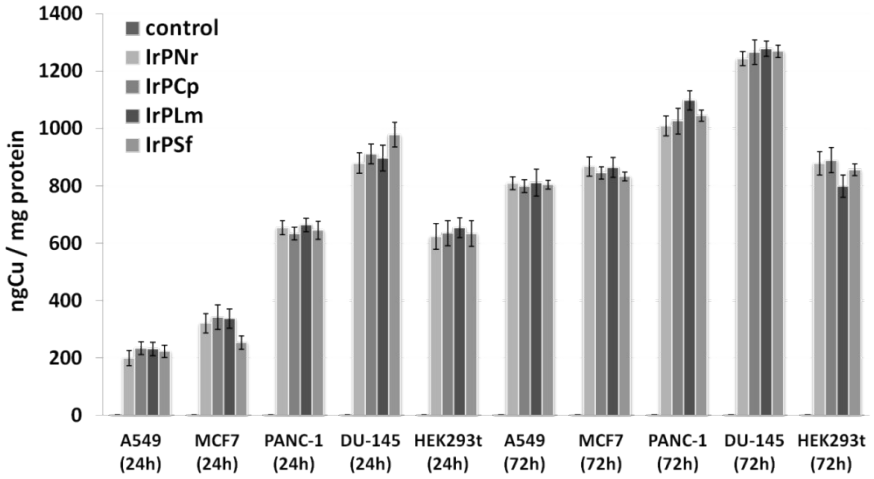

Fig. S24. Time-dependency of final intracellular iridium concentration expressed as ng Ir per mg protein after 24h and 24h* (24h + 48h) of incubation with the A549, MCR7, PANC-1, DU-145 and HEK293T cell lines for IrPCp, IrPNr, IrPSf, IrPLm complexes in c = 1 μM.

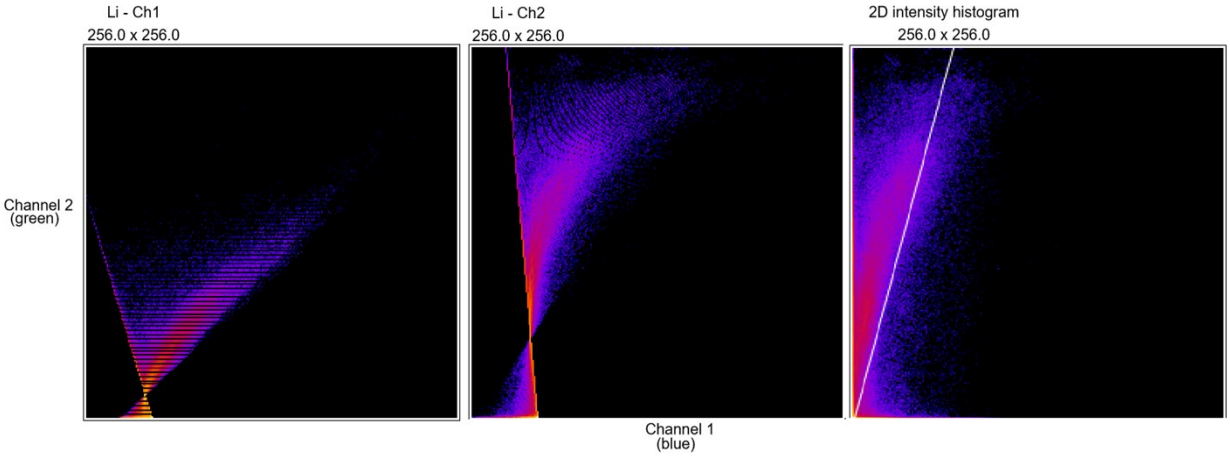

Fig. S25. Co-localization analysis performed with ImageJ plugin - Coloc2 which implements and performs the pixel intensity correlation over space.

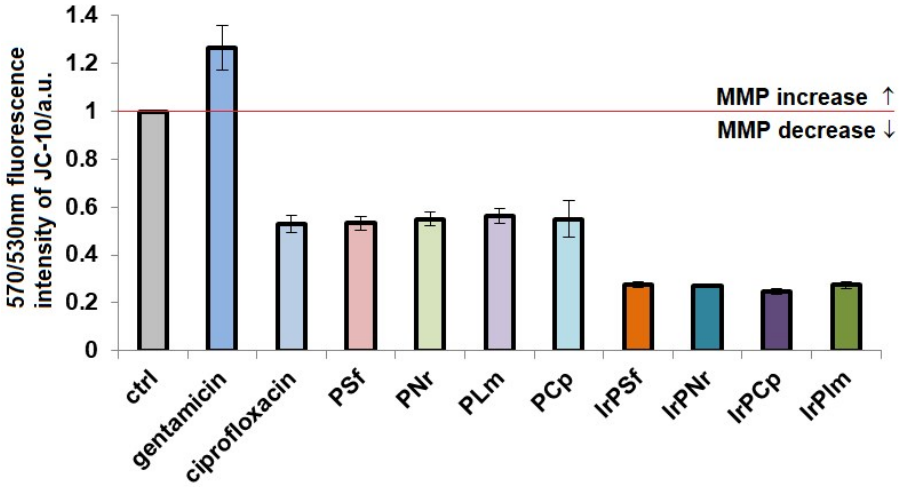

Fig. S26. Influence of studied complexes (IC_{50}) on intensity of JC-10 fluorescence in treated DU-145 cells. Alteration in MMP is given as an emission ratio 570 nm/530 nm. (ctrl – untreated cells, ciprofloxacin – a negative control, gentamicin – a positive control).

Table S5. Hydrodynamic diameter and Zeta potential determined by DLS technique as well as loading content and encapsulation efficiency determined by ICP-MS technique for selected Pluronic P-123 formulations.

Formulation	Hydrodynamic diameter [nm]	Zeta potential	LC ± S.D. [%]	EE ± S.D. [%]
IrPCp_M	19 ± 1 (PDI = 0.5 ± 0.1)	-1.5 ± 0.4	19.5 ± 2.9	99.5 ± 1.2
IrPNr_M	18 ± 2 (PDI = 0.4 ± 0.1)	-1.6 ± 0.3	29.8 ± 2.2	98.0 ± 0.5

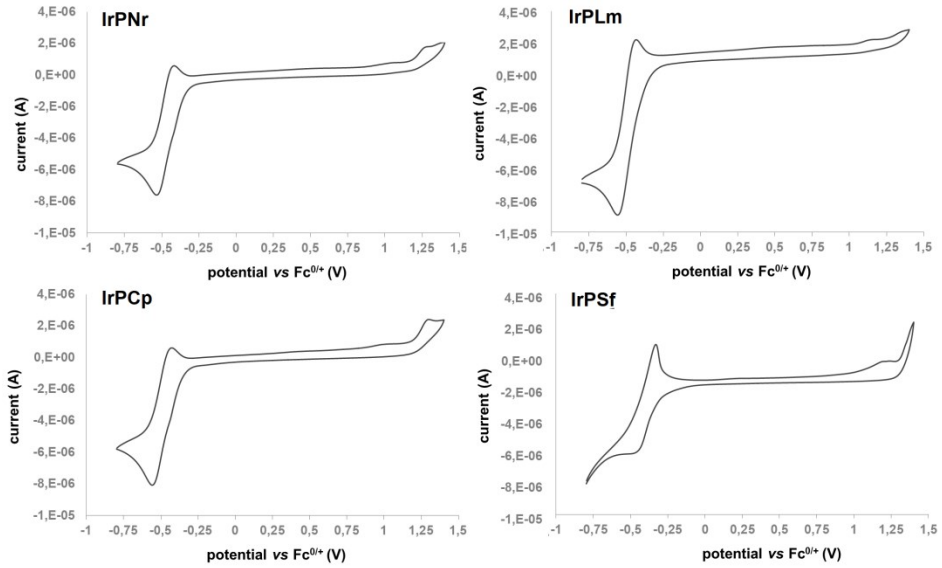

Fig. S27. Cyclic voltammograms of iridium(III) complexes (1 mM), recorded with 0.1 M tetrabutyl ammonium perchlorate (TBAP) as supporting electrolyte in DMF solution. Scan rates (10 mVs^{-1}). The potentials were referenced to the $Fc^{0/+}$ redox couple.

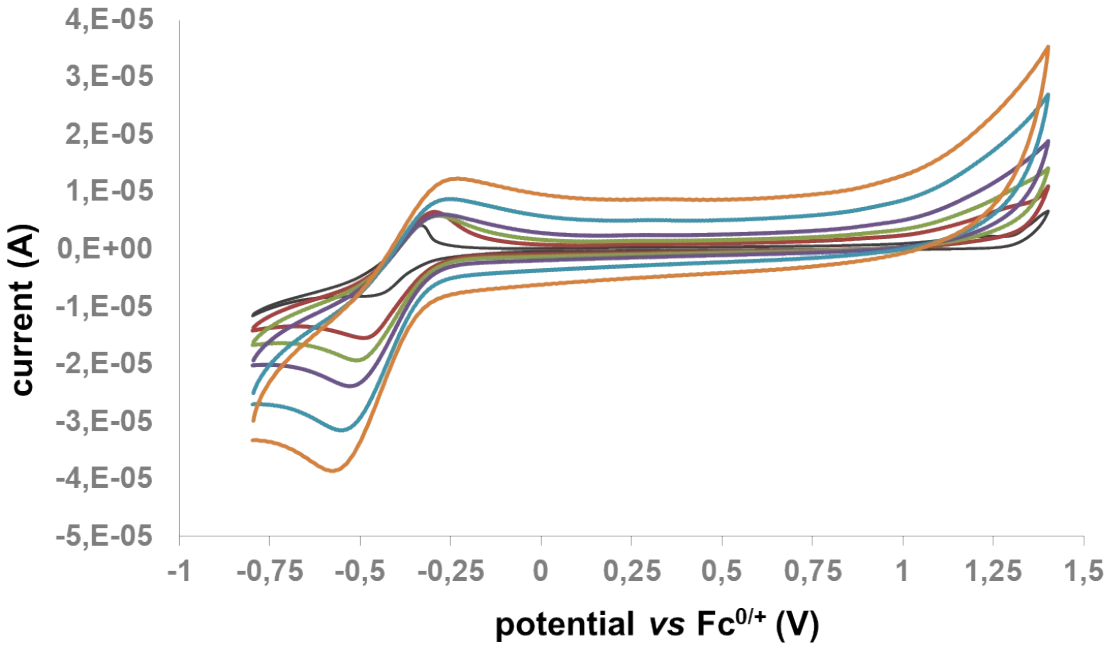

Fig. S28. Cyclic voltammetric trace of **IrPSf**(1 mM) as a function of scan rate, recorded with recorded with 0.1 M tetrabutyl ammonium perchlorate (TBAP) as supporting electrolyte in DMF solution. Scan rates 1 – 100 (mV s^{-1}). Potential (V) versus $Fc^{0/+}$.

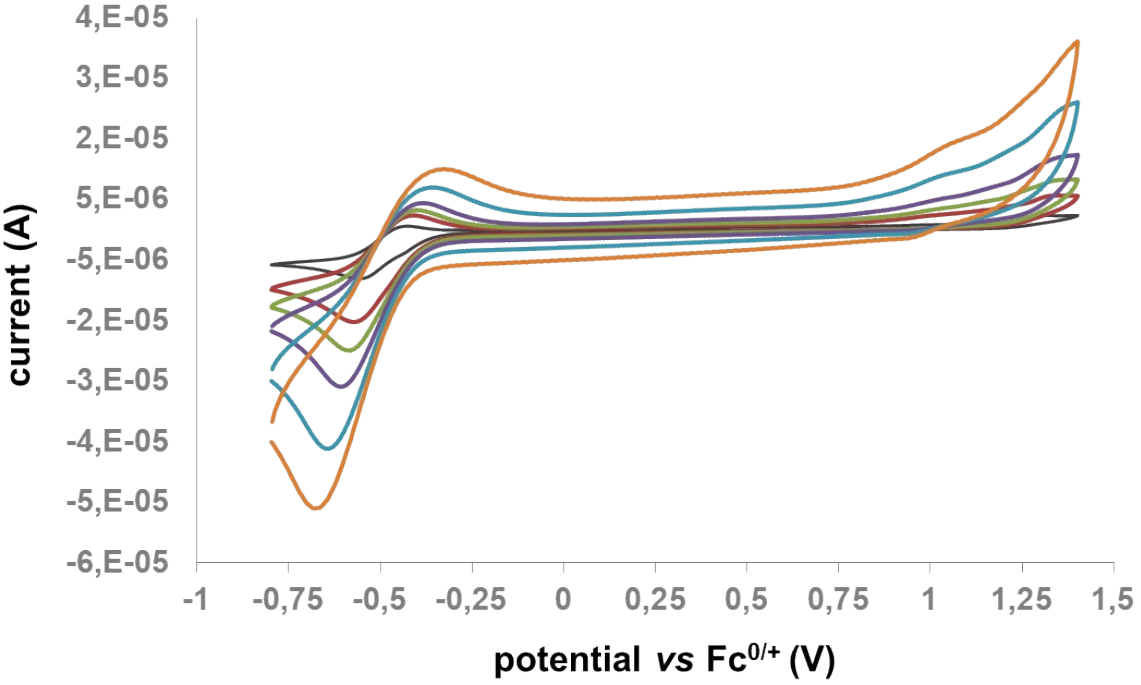

Fig. S29. Cyclic voltammetric trace of **IrPCp**(1 mM) as a function of scan rate, recorded with recorded with 0.1 M tetrabutyl ammonium perchlorate (TBAP) as supporting electrolyte in DMF solution. Scan rates 1 – 100 (mV s^{-1}). Potential (V) versus $Fc^{0/+}$.

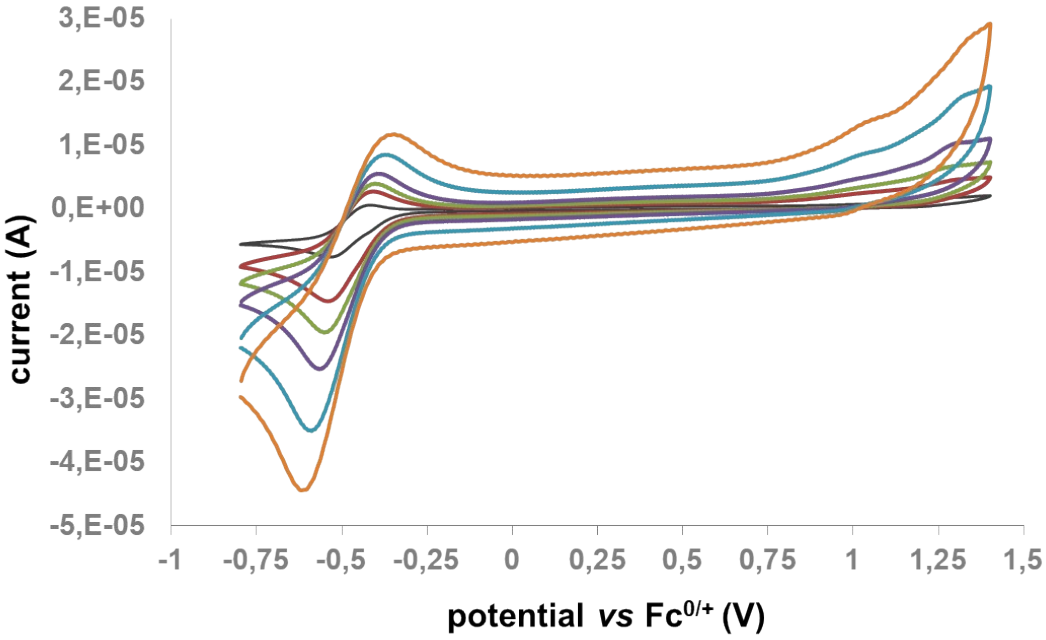

Fig. S30. Cyclic voltammetric trace of **IrPCp**(1 mM) as a function of scan rate, recorded with recorded with 0.1 M tetrabutyl ammonium perchlorate (TBAP) as supporting electrolyte in DMF solution. Scan rates 1 – 100 (mV s^{-1}). Potential (V) versus $Fc^{0/+}$.

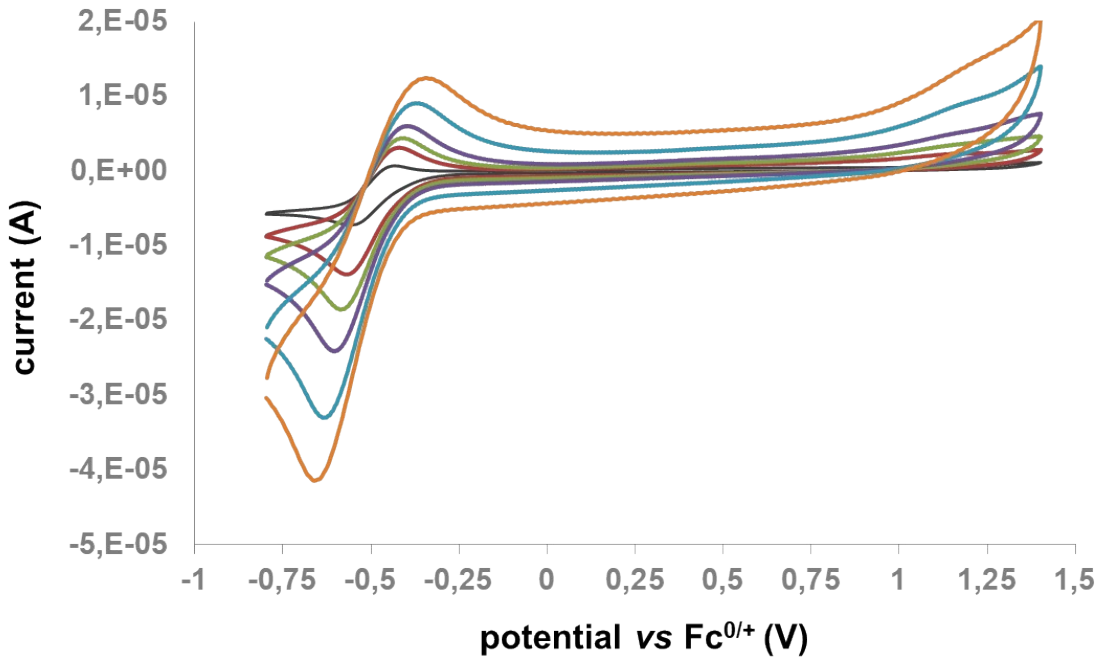

Fig. S31. Cyclic voltammetric trace of **IrPCp**(1 mM) as a function of scan rate, recorded with recorded with 0.1 M tetrabutyl ammonium perchlorate (TBAP) as supporting electrolyte in DMF solution. Scan rates 1 – 100 (mV s^{-1}). Potential (V) versus $Fc^{0/+}$.

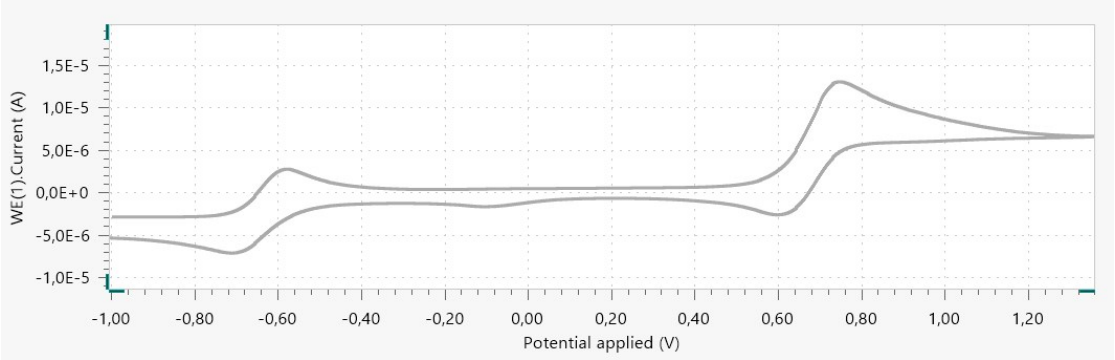

Fig. S32. CVvoltammograms for ferrocene in DMF in the range of potentials from -01 V to 1.2 V. Scan rate: 10 mV s^{-1}.